Published OnlineFirst April 2, 2013; DOI: 10.1158/1535-7163.MCT-13-0065

Molecular Cancer Therapeutics

# Synergistic Anticancer Activity of Arsenic Trioxide with Erlotinib Is Based on Inhibition of EGFR-Mediated DNA Double-Strand Break Repair

Kushtrim Kryeziu, Ute Jungwirth, Mir Alireza Hoda, et al.

*Mol Cancer Ther* Published OnlineFirst April 2, 2013.

Published OnlineFirst April 2, 2013; DOI: 10.1158/1535-7163.MCT-13-0065

*Cancer Therapeutics Insights*

Molecular Cancer Therapeutics

# Synergistic Anticancer Activity of Arsenic Trioxide with Erlotinib Is Based on Inhibition of EGFR-Mediated DNA Double-Strand Break Repair

Kushtrim Kryeziu[1,2,3], Ute Jungwirth[1,2,3], Mir Alireza Hoda[1,2], Franziska Ferk[1,2], Siegfried Knasmüller[1,2], Claudia Karnthaler-Benbakka[3,4], Christian R. Kowol[3,4], Walter Berger[1,2,3], and Petra Heffeter[1,2,3]

## Abstract

Arsenic trioxide (ATO), one of the oldest remedies used in traditional medicine, was recently rediscovered as an anticancer drug and approved for treatment of relapsed acute promyelocytic leukemia. However, its activity against nonhematologic cancers is rather limited so far. Here, we show that inhibition of ATO-mediated EGF receptor (EGFR) activation can be used to potently sensitize diverse solid cancer types against ATO. Thus, combination of ATO and the EGFR inhibitor erlotinib exerted synergistic activity against multiple cancer cell lines. Subsequent analyses revealed that this effect was based on the blockade of ATO-induced EGFR phosphorylation leading to more pronounced $G_2$–M arrest as well as enhanced and more rapid induction of apoptosis. Comparable ATO-sensitizing effects were also found with PI3K/AKT and mitogen-activated protein/extracellular signal–regulated kinase (MEK) inhibitors, suggesting an essential role of the EGFR-mediated downstream signaling pathway in cancer cell protection against ATO. H2AX staining and comet assay revealed that erlotinib significantly increases ATO-induced DNA double-strand breaks (DSB) well in accordance with a role of the EGFR signaling axis in DNA damage repair. Indeed, EGFR inhibition led to downregulation of several DNA DSB repair proteins such as Rad51 and Rad50 as well as reduced phosphorylation of BRCA1. Finally, the combination treatment of ATO and erlotinib was also distinctly superior to both monotreatments against the notoriously therapy-resistant human A549 lung cancer and the orthotopic p31 mesothelioma xenograft model *in vivo*. In conclusion, this study suggests that combination of ATO and EGFR inhibitors is a promising therapeutic strategy against various solid tumors harboring wild-type EGFR. *Mol Cancer Ther; 12(6); 1–12. ©2013 AACR.*

## Introduction

In 2000, arsenic trioxide (ATO; Fig. 1A) was approved by the U.S. Food and Drug Administration for the treatment of relapsed and refractory acute promyelocytic leukemia (APL; ref. 1) and, thus, represents besides platinum compounds the only metal-based anticancer drug in clinical use. Induction of intracellular reactive oxygen species (ROS) and reactive nitrogen species (RNS) based on interference with the intracellular redox balance is one of the main mechanisms of action underlying the anticancer activity of ATO (1, 2). In addition, the selective efficacy of ATO against APL was shown to be due to degradation of the APL-specific promyelocytic leukemia and retinoic acid receptor-α (PML-RARα) fusion oncoprotein (3, 4). On the basis of its successful clinical application, the anticancer activity of ATO either as monotreatment or in combination with other agents was also intensively studied in various other hematologic malignancies (5, 6) and several solid cancer types (7). However, reports from phase II clinical trials on patients with hepatocellular carcinoma (HCC), metastatic renal cell carcinoma, and metastatic melanoma suggested so far that ATO has only limited efficacy against solid tumors (8–12). Although multiple resistance mechanisms for arsenic have been described on the cellular level (1), the reasons underlying the lack of efficacy of ATO in solid tumor types are still widely unclear.

In addition to its use as anticancer agent, arsenic came into the focus of interest as unintentional exposure to inorganic arsenic salts (mainly via drinking water) was found to exert potent carcinogenic activity (13). Recently, arsenic was reported to induce activation of the EGF receptor (EGFR) pathway in nonmalignant tissues of exposed humans (such as lung, bladder, and prostate;

**Authors' Affiliations:** [1]Department of Medicine I, Institute of Cancer Research; [2]Comprehensive Cancer Center, Medical University Vienna; [3]Research Platform "Translational Cancer Therapy Research"; and [4]Institute of Inorganic Chemistry, University of Vienna, Vienna, Austria

**Note:** Supplementary data for this article are available at Molecular Cancer Therapeutics Online (http://mct.aacrjournals.org/).

**Corresponding Authors:** Petra Heffeter, Department of Medicine I, Institute of Cancer Research, Medical University Vienna, Borschkegasse 8a, 1090 Vienna, Austria. Phone: 43-1-40160-57557; Fax: 43-1-40160-957555; E-mail: petra.heffeter@meduniwien.ac.at; and Walter Berger, walter.berger@meduniwien.ac.at

**doi:** 10.1158/1535-7163.MCT-13-0065

Published OnlineFirst April 2, 2013; DOI: 10.1158/1535-7163.MCT-13-0065



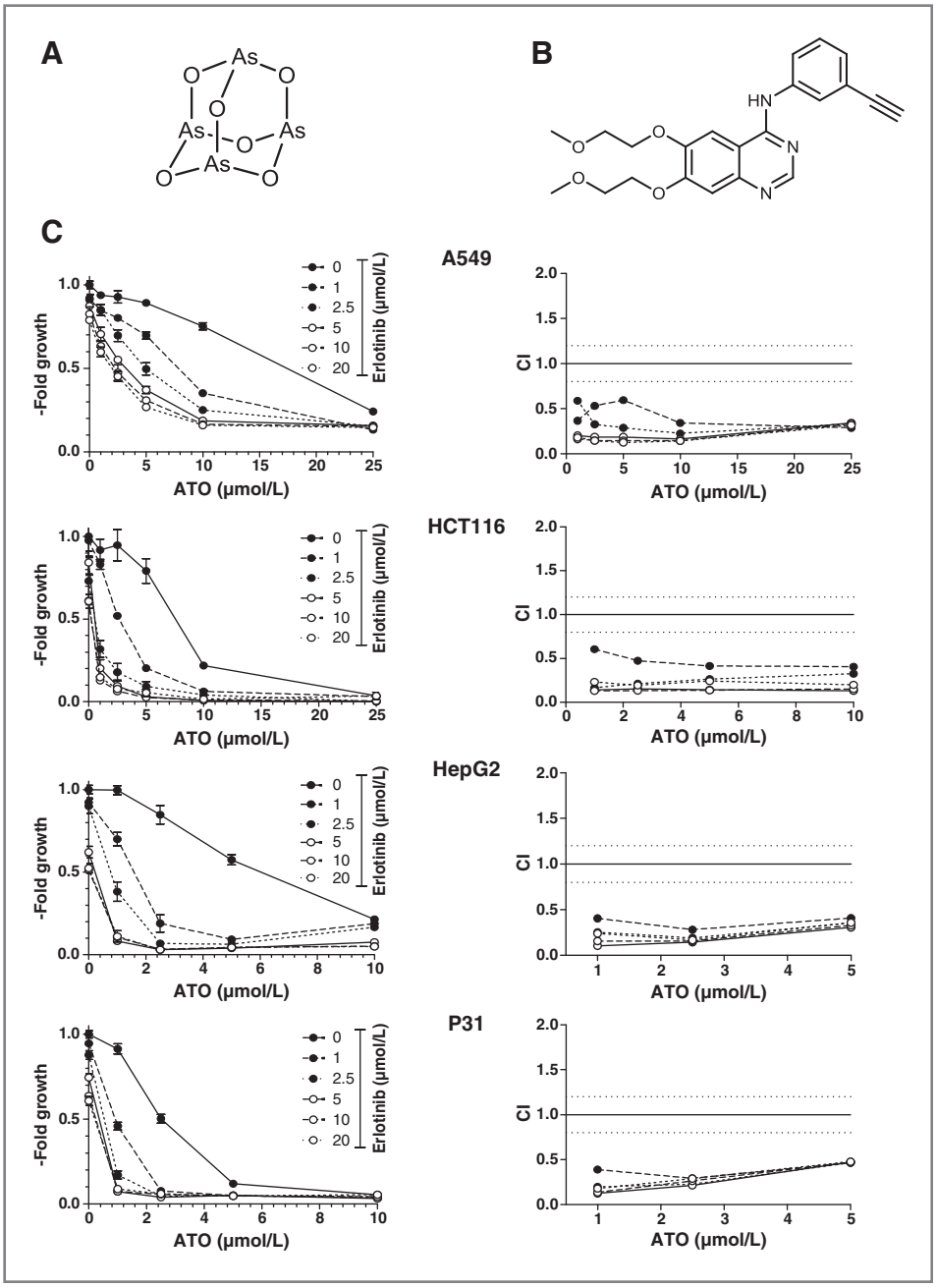


**Figure 1.** Impact of ATO in combination with erlotinib after 72-hour continuous exposure on the viability of the indicated cancer cell lines. Chemical structures of ATO (A) and erlotinib (B). C, the diagrams on the left show viability changes as compared with the untreated control measured by MTT assay. Respective isobolograms on the right depict CIs calculated following the method of Chou and Talalay by using CalcuSyn Software. All experiments were carried out in triplicate and repeated at least 3 times.

refs. 14, 15). Consequently, this EGFR response was suggested to be one of the main drivers of the carcinogenic effect of inorganic arsenic salts (16). In addition, stimulation of EGFR was also observed in several malignant cancer types after treatment with arsenic (17, 18). The mechanisms underlying the recently described stimulation of EGFR by arsenic are still a matter of discussion. On the one hand, treatment with arsenic might stimulate the release of the EGFR ligand, heparin-binding EGF (19). On the other hand, the metal was shown to induce c-Src, which subsequently phosphorylates the EGFR (18, 20).

With regard to cancer, the EGFR pathway is a major player in cell survival, cell-cycle progression, tumor invasion, and angiogenesis (21). Moreover, there are several reports that the stimulation of the EGFR pathway is associated with enhanced DNA damage repair (22). Thus, based on the importance of the EGFR signaling for cell survival in malignant tissues and the discovery of several mutations leading to constitutive EGFR activation (23), this pathway was identified as an ideal target for cancer treatment. Consequently, several EGFR inhibitors have already been successfully developed and approved for the treatment of solid human malignancies especially

Published OnlineFirst April 2, 2013; DOI: 10.1158/1535-7163.MCT-13-0065



non–small cell lung carcinoma (NSCLC) at the disseminated stage (e.g., erlotinib, gefitinib; ref. 23).

On the basis of the known EGFR stimulation by environmental arsenic exposure and the role of EGFR-mediated signals in multiple survival pathways, we hypothesized that EGFR might be involved in the insensitivity of solid tumors to ATO treatment. Consequently, the aim of the present study was to investigate the effects of erlotinib (Fig. 1B) on the anticancer activity of ATO against diverse solid cancer types and to gain more insights into the underlying molecular mechanisms.

## Materials and Methods

### Chemicals

ATO was purchased from Sigma-Aldrich, gefitinib from AstraZeneca, MK-2206 from Selleck Chemicals LLC, U0126 from Cell Signaling, and all other kinase inhibitors were from LC laboratories. For *in vitro* studies, ATO was dissolved in 1 mol/L NaOH, whereas for all other substances dimethyl sulfoxide (DMSO) stocks were prepared. The stock solutions were further diluted into culture media at the indicated concentrations. The final DMSO and NaOH concentrations were always less than 1%.

### Cell culture

The following human cancer cell lines were used in this study: the NSCLC cell lines A549 and A427 [from American Type Culture Collection (ATCC)]; the mesothelioma cell line P31 (donated by Prof. K. Grankvist, Umeå University, Umeå, Sweden); the mesothelioma cell lines VMC6, VMC12, VMC23, and VMC31 (established at the Institute of Cancer Research, Vienna, Austria); the HCC HepG2 (from ATCC); the colorectal carcinoma cell lines HCT116 (donated by Dr. B. Vogelstein, John Hopkins University, Baltimore, MD), SW620 and SW480 (from ATCC); osteosarcoma cell lines IOS (donated by Dr. Manara, Istituti Ortopedici Rizzoli, Bologna, Italy) and MG63 (from ATCC); the thyroid carcinoma cell lines SW1736 and SW579 (from ATCC); and the cervix carcinoma KB-3-1 (donated by Dr. Shen, Laboratory of Cell Biology, National Cancer Institute, National Institutes of Health, Bethesda, MD). HCT116 cells were grown in McCoy's culture medium. A427, HepG2, SW480, and P31 were grown in minimum essential medium. All other cell lines were cultivated in RPMI-1640. Culture media were supplemented with 10% fetal calf serum (PAA). Cell cultures were periodically checked for *Mycoplasma* contamination. Cell line authentication has been done either by array-comparative genomic hybridization and/or short tandem repeat fingerprint.

### Cytotoxicity assays

Cells were plated ($2 \times 10^3$ cells/well) in 96-well plates and allowed to recover for 24 hours. Subsequently, the dissolved drugs were added. After 72-hour exposure, the proportion of viable cells was determined by MTT assay following the manufacturer's recommendations (EZ4U; Biomedica). Cytotoxicity was expressed as $IC_{50}$ values calculated from full dose–response curves. Synergism was determined by calculation of the combination index (CI) according to Chou and Talalay (24) using the CalcuSyn software (Biosoft). CI < 0.8, CI = 0.8–1.2, or CI > 1.2 represent synergism, additive effects, and antagonism of the 2 investigated substances, respectively.

### Cell-cycle analysis

Cells ($2 \times 10^5$) were seeded into 6-well plates and allowed to recover for 24 hours. After drug exposure, cells were collected, washed with PBS, fixed in 70% ice-cold ethanol, and stored at −20°C. To analyze cell-cycle distribution, cells were transferred into PBS, incubated with RNAse A (10 μg/mL) for 30 minutes at 37°C, followed by 30-minute treatment with 5 μg/mL propidium iodide (PI). Fluorescence levels were analyzed by flow cytometry using FACSCalibur (Becton Dickinson). The resulting DNA histograms were quantified using Cell Quest Pro software (Becton Dickinson and Company).

### Mitochondrial membrane potential detection

Breakdown of the mitochondrial membrane potential ($\Delta\Upsilon_m$) was determined by fluorescence-activated cell sorting (FACS) analysis using JC-1 (5,5′,6,6′-tetrachloro-1,1′,3,3′-tetraethylbenzimidazol-carbocyanine iodide). For this purpose, the Mitochondrial Membrane Potential Detection Kit (Stratagene) was used according to the manufacturer's instructions. A549 cells ($5 \times 10^5$) were seeded in T25 $cm^2$ culture flasks and treated with the tested drugs after 24-hour recovery. After trypsinization and PBS washing, cells were incubated for 10 minutes in freshly prepared JC-1 solution (10 μg/mL in cell culture media) at 37°C. Spare dye was removed by washing in PBS and cell-associated fluorescence measured via FACS.

### Hoechst 33258–PI staining

A549 cells ($2 \times 10^4$ cells/well) were seeded in 24-well plates and allowed to recover for 24 hours. Cells were treated with ATO and erlotinib for the indicated exposure times. Then, the cells were stained with 2 μL/mL HOEPI mix [ratio 1:1—Hoechst 33258 (1 mg/mL) and PI (2.5 mg/mL)] for 1 hour at 37°C. Live photomicrographs of treated cells were made using fluorescent equipment on the Nikon Eclipse Ti inverted microscope system. Triplicate photomicrographs for each treatment were captured with 4′,6-diamidino-2-phenylindole (DAPI)-, CY3-filters, and phase contrast. Morphologic features of more than 300 cell nuclei for each treatment were counted.

### $^3$H-thymidine incorporation assay

A549 cells ($5 \times 10^3$ cells/well) were seeded in a 96-well plate and treated 24 hours later with drugs for another 24 hours. Medium was replaced by a 2 nmol/L $^3$H-thymidine solution (diluted in full culture medium; radioactivity: 25 ci/mmol/L). After 1-hour incubation at 37°C, cells were washed 3 times with PBS. Cell lysates were prepared and the radioactivity determined as described previously (25).

Published OnlineFirst April 2, 2013; DOI: 10.1158/1535-7163.MCT-13-0065



### Western blot analysis

Proteins were isolated, resolved by SDS/PAGE, and transferred onto a polyvinylidene difluoride membrane for Western blotting as previously described (26). The following antibodies were used: EGFR, pEGFR (Tyr992 and Tyr1068), AKT, pAKT (Ser437), extracellular signal–regulated kinase (ERK)1/2 [p44/42 mitogen-activated protein kinase (MAPK)], pERK (Thr202/Tyr204), pH2AX (Ser139), cyclin B1, Rad50, Rad51, pBRCA1 (Ser1524), PARP, cl. PARP, and p21 Waf/Cip1 (all polyclonal rabbit; Cell Signaling Technology), p53 (DO-1; monoclonal mouse; Thermo Scientific), β-actin and α-tubulin monoclonal mouse AC-15 (Sigma) were all used in 1:1,000 dilutions. In addition, horseradish peroxidase–labeled secondary antibodies from Santa Cruz Biotechnology were used at working dilutions of 1:10,000.

### Immunofluorescence

A total of $2 \times 10^4$ A549 cells were seeded in 8-well chamber slides (BD Falcon). After 24 hours recovery cells were treated for another 24 hours with ATO, erlotinib, and their combination. Treated cells were washed with PBS and fixed in methanol/acetone at 4°C for 10 minutes before washing 3 times for 10 minutes in PBS with 1% bovine serum albumin (BSA). Fixed cells were incubated with phospho-H2AX antibody [diluted 1:100 in PBS with 1% BSA (Cell signaling)] for 1 hour at room temperature. After 3 further washing steps with PBS (1% BSA), cells were incubated (1 hour) with the second antibody (anti-rabbit immunoglobulin G (IgG) labeled with fluorescein isothiocyanate (FITC); Sigma-Aldrich), diluted 1:1,000 in PBS with 1% BSA. Cells were counterstained with DAPI before mounting. Images were obtained using a Leica DMRXA fluorescence microscope (Leica Mikroskopie und System) equipped with appropriate epifluorescence filters and a COHU charge-coupled device camera. Subsequent image handling was carried out in Adobe Photoshop CS4.

### Comet assay

DNA double-strand breaks (DNA DSB) were analyzed using alkaline comet assay according to the guidelines of Tice and colleagues (27). A549 cells were seeded in 6-well plates ($2.5 \times 10^5$ cells/well) and allowed to recover for 24 hours. After treatment for 6 hours, cells were trypsinized and washed with PBS. Cells treated with 100 μmol/L $H_2O_2$ were trypsinized after 30 minutes. Comet assay was then conducted with some modifications as described by Heffeter (28).

### Animals

Six- to 8-week-old female CB-17 scid/scid [severe combined immunodeficient mice (SCID)] mice were purchased from Harlan Laboratories. The animals were kept in a pathogen-free environment and every procedure was done in a laminar airflow cabinet. The experiments were carried out according to the regulations of the Ethics Committee for the Care and Use of Laboratory Animals at the Medical University Vienna (Vienna, Austria), the U.S. Public Health Service Policy on Human Care and Use of Laboratory Animals as well as the United Kingdom Coordinating Committee on Cancer Prevention Research's Guidelines for the Welfare of Animals in Experimental Neoplasia.

### Xenograft experiments

For the local tumor growth experiments, A549 cells ($1 \times 10^6$) were injected subcutaneously into the right flank. For orthotropic models, P31 cells ($6 \times 10^6$) were injected intraperitoneally. Animals were randomly assigned to treatment groups and therapy was started when tumor nodules reached a mean size of 25 $mm^3$ (A549) or 1 week after injection (P31). Animals were treated with erlotinib (orally 25 mg/kg dissolved in Cremophor EL diluted 1:1 in 96% ethanol and then diluted 1:10 with deionized water right before administration; 5 times a week for 2 weeks), ATO [intraperitoneally (i.p.) 5 mg/kg dissolved in 1 mol/L NaOH and further diluted in PBS 1:10. pH value was adjusted at 7.0–7.5 with HCl before administration; 5 times a week for 2 weeks], or with a combination of both drugs. Animals in the control group received the Cremophor EL solvent orally and PBS intraperitoneally. Animals were controlled for distress development every day and tumor size was assessed regularly by caliper measurement (A549). Tumor volume was calculated using the formula: (length × $width^2$)/2. P31 tumors were weighted after mice were sacrificed. The P31 experiment was terminated after 62 days from transplantation when the first animal had to be sacrificed because of weight loss as previously shown in Hoda and colleagues (29).

### Statistical analysis

All data are expressed as mean ± SD. Results were analyzed and illustrated with GraphPad Prism (version 5; GraphPad Software). Statistical analyses were performed using one- and two-way ANOVA with drug treatment and time as independent variables and conducted with Bonferroni posttests to examine the differences between the different drug treatment regimens and the diverse responses. The statistical significance is either described in the respective figure legends, or indicated with asterisks (*, $P < 0.05$; **, $P < 0.01$; ***, $P < 0.001$).

## Results

### ATO and erlotinib synergistically reduce cancer cell viability

The cell lines used in this study and their respective $IC_{50}$ values after 72-hour treatment with ATO and erlotinib (as single agents or combined) are listed in Table 1. In addition, genetic characteristics are shown in Supplementary Table S1. Selected full dose–response curves are shown in Fig. 1C and in Supplementary Fig. S1A–S1C. ATO monotreatment exerted distinct anticancer activity against the tested cells in the low μmol/L range. The most resistant cell lines were IOS (osteosarcoma; $IC_{50} > 25$ μmol/L), VMC31 (mesothelioma; $IC_{50} = 18.87$ μmol/L),

Published OnlineFirst April 2, 2013; DOI: 10.1158/1535-7163.MCT-13-0065



**Table 1.** $IC_{50}$ values of different cells treated with ATO, erlotinib, or their combination

| Cell line | Histology | ATO (μmol/L) $IC_{50}$ | Erlotinib (μmol/L) $IC_{50}$ | ATO with 2.5 μmol/L Erlo $IC_{50}$ | Fold decrease[a] |
|---|---|---|---|---|---|
| A427 | NSCLC | 5.2 ± 0.4 | >20 | 4.5 ± 0.3 | 1.2 |
| A549 | NSCLC | 17.6 ± 0.9 | >20 | 5.7 ± 0.8 | 3.1 |
| HepG2 | HCC | 5.9 ± 0.7 | >20 | 0.8 ± 0.1 | 7.4 |
| HCT116 | CC | 7.5 ± 0.3 | >20 | 0.8 ± 0.1 | 9.4 |
| SW480 | CC | 8.6 ± 0.1 | >20 | 2.8 ± 0.2 | 3.1 |
| SW620 | CC | 8.4 ± 0.3 | >20 | 4.2 ± 0.1 | 2.0 |
| IOS | OS | >25 | >20 | 9.3 ± 0.1 | >2.7 |
| MG63 | OS | 2.8 ± 0.1 | >20 | 1.2 ± 0.1 | 2.3 |
| KB-3-1 | Cervical carcinoma | 6.3 ± 0.3 | >20 | 2.0 ± 0.1 | 3.2 |
| SW579 | TC | 1.9 ± 0.1 | >20 | 0.8 ± 0.1 | 2.4 |
| SW1736 | TC | 8.5 ± 0.1 | >20 | 4.7 ± 0.1 | 1.8 |
| P31 | Mesothelioma | 2.5 ± 0.1 | >20 | 0.5 ± 0.1 | 5.0 |
| VMC6 | Mesothelioma | 11.8 ± 0.1 | >20 | 4.4 ± 0.3 | 2.7 |
| VMC12 | Mesothelioma | 11.3 ± 0.3 | >20 | 3.4 ± 0.1 | 3.3 |
| VMC23 | Mesothelioma | 12.3 ± 0.2 | 16.9 ± 0.2 | 4.7 ± 0.3 | 2.6 |
| VMC31 | Mesothelioma | 18.9 ± 0.2 | >20 | 4.8 ± 0.2 | 3.9 |

Abbreviations: CC, colon carcinoma; OS, osteosarcoma; TC, thyroid carcinoma.

[a]Fold decrease of ATO $IC_{50}$ calculated by dividing $IC_{50}$ of ATO alone by $IC_{50}$ of ATO with 2.5 μmol/L erlo.

and A549 (NSCLC; $IC_{50} = 17.58$ μmol/L), whereas SW579 (thyroid carcinoma; $IC_{50} = 1.95$ μmol/L), MG63 (osteosarcoma; $IC_{50} = 2.87$ μmol/L), and P31 (mesothelioma; $IC_{50} = 2.52$ μmol/L) exhibited the strongest ATO sensitivity. As all cell lines harbor wild-type EGFR, the anticancer effect of erlotinib was minor and resulted in general in $IC_{50}$ values above 20 μmol/L (Table 1).

Combination of ATO and erlotinib had synergistic activities as compared with monotherapy with ATO (up to 9.4-fold decrease in $IC_{50}$ values in case of HCT116). In general, synergistic CI values less than 0.6 were observed at low erlotinib concentrations (1–2.5 μmol/L), which became more pronounced at higher erlotinib concentrations (5–20 μmol/L) leading to CI values $\leq 0.05$. Notably, no antagonistic effects were observed in any of the tested cell lines. To investigate whether a synergistic activity with ATO is also observed with other EGFR inhibitors, combinations with gefitinib (EGFR) and lapatinib (EGFR and HER2/neu) were tested. As can be seen in Fig. 2A and B, the anticancer activity of ATO was also synergistically increased by these inhibitors, especially at higher concentrations of gefitinib (CI < 0.1; Fig. 2A).

### Erlotinib inhibits ATO-induced EGFR stimulation

To investigate whether, in accordance to other studies (15–19), treatment with ATO leads to induction of EGFR signaling, the EGFR phosphorylation status of ATO-treated A549 cells was analyzed by Western blotting. This cell line was selected, as it is known for its notorious drug resistance against multiple chemotherapeutics. As presented in Fig. 2C and Supplementary Fig. S2A, respectively, ATO time- and dose-dependently increased EGFR phosphorylation at Y1068 and Y992 sites with the most pronounced phosphorylation detected after 16 hours. Notably, also in the case of erlotinib, a slight increase of EGFR phosphorylation was detected at the Y992 but not the Y1068 site. Treatment with erlotinib completely inhibited ATO-induced EGFR phosphorylation at both analyzed tyrosine sites (Y1068 and Y922).

### ATO synergizes with inhibitors of the EGFR downstream signaling

EGFR signaling is known to result in the activation of the MAPK and the PI3K/AKT kinase pathways (23). To gain more insights into the role of these EGFR downstream signaling pathways in the synergistic effects of ATO with erlotinib, the phosphoinositide 3-kinase (PI3K)-inhibitor Ly294002 and the AKT-inhibitor MK-2206 were used to block the PI3K/AKT pathway, whereas for the MAPK pathway the mitogen-activated protein/extracellular signal–regulated kinase (MEK)-inhibitor U0126 was applied (Fig. 2D–F and Supplementary Fig. S2B–S2D). Notably, strong synergism was observed by combination of ATO with all 3 kinase inhibitors with CI values between 0.73 and 0.02 for MK-2206, 0.93 and 0.3 for Ly294002, and 0.9 and 0.1 for U0126. With regard to pathway stimulation, ATO monotreatment induced phosphorylation of AKT (in accordance to Liu and colleagues, ref. 30), which was inhibited by cotreatment with erlotinib as well as both inhibitors of the PI3K/AKT pathway (Fig. 2D and E, bottom). Notably, no stimulation of ERK phosphorylation by ATO monotreatment was observed (Fig. 2F, bottom). However, although ATO monotreatment had no visible effect on the ERK phosphorylation status, the combination

Published OnlineFirst April 2, 2013; DOI: 10.1158/1535-7163.MCT-13-0065



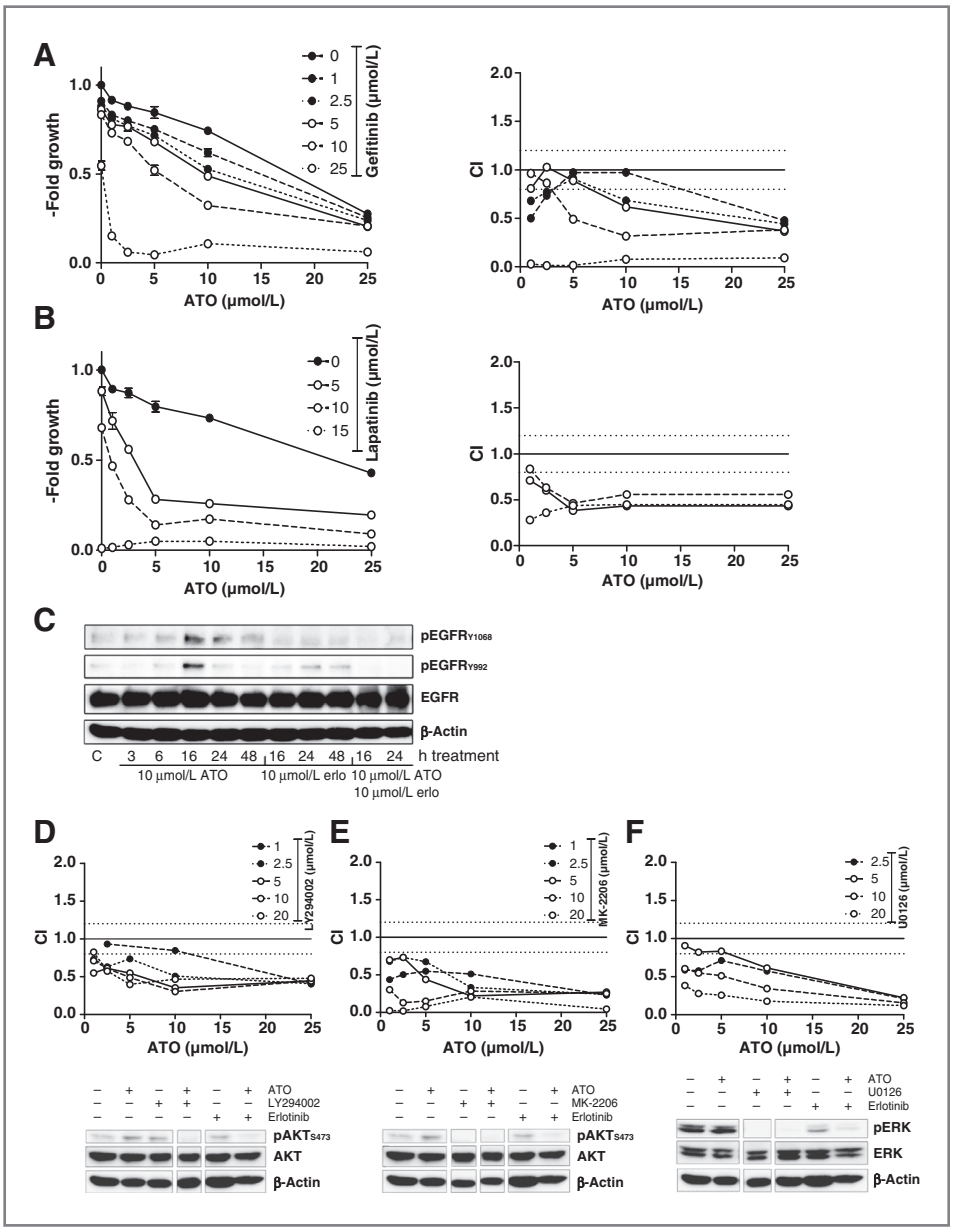


**Figure 2.** Impact of ATO in combination with inhibitors of EGFR and downstream signaling. Anticancer effects of ATO cotreatment with gefitinib (A) and lapatinib (B) on the viability of A549 NSCLC cells: viability diagrams (left) and the respective CI values (right) at indicated concentrations. C, impact of ATO, erlotinib (erlo), and their combination on EGFR phosphorylation of A549 cells. Western blot analysis of EGFR phosphorylation after 3-, 6-, 16-, 24-, and 48-hour treatment with ATO, erlotinib, or their combination. Anticancer activity of the PI3K inhibitor LY294002 (D), the AKT inhibitor MK-2206 (E), and the MEK inhibitor U0126 (F) in combination with ATO was tested against A549 cells. Viability was measured by MTT assay after 72-hour drug exposure. CIs and Western blot analyses of AKT and ERK phosphorylation after treatment (24 hours) of ATO combined with LY294002, MK-2206, U0126, and erlotinib are shown. Phosphorylation of AKT and ERK served as parameter for the activity of PI3K/AKT pathway and MAPK pathway inhibitors, respectively. (For Western blot analyses 10 μmol/L of each drug were used).

with erlotinib further enhanced the erlotinib-induced ERK inhibition indicating that ATO also modulates the anticancer activity of erlotinib.

### Effects of erlotinib on ATO-induced apoptosis and cell-cycle arrest

In a next step, it was investigated whether the observed synergism was due to enhanced apoptosis induction or the inhibition of cell proliferation (Fig. 3A). Notably, no increase of apoptosis rates was observed after 24-hour drug exposure in any of the experimental groups (Supplementary Fig. S3A and S3B). Also, after 48 hours, no induction of programmed cell death was observed in A549 cells treated with either ATO or erlotinib monotreatment. In contrast, combination of the 2 drugs resulted in up to 10-fold raise of the apoptosis levels (Supplementary Fig. S3C). This effect was further increased after 72-hour drug exposure leading to up to 90% PI-positive cells in the highest combination setting (10 μmol/L of each drug; Fig. 3B). This time-dependent effect was confirmed by detection of caspase-dependent PARP cleavage (Fig. 3C).

To investigate whether ATO in combination with erlotinib influences DNA synthesis, $^{3}$H-thymidine incorporation assays were conducted (Fig. 3F). After 24-hour incubation, only a slight decrease of DNA synthesis was detected after ATO monotreatment, whereas 5 and 10 μmol/L erlotinib blocked replication by 22% and 43%, respectively. In contrast, ATO cotreatment with erlotinib induced a strong synergistic decrease of $^{3}$H-thymidine incorporation at all concentrations resulting in CI values

Published OnlineFirst April 2, 2013; DOI: 10.1158/1535-7163.MCT-13-0065



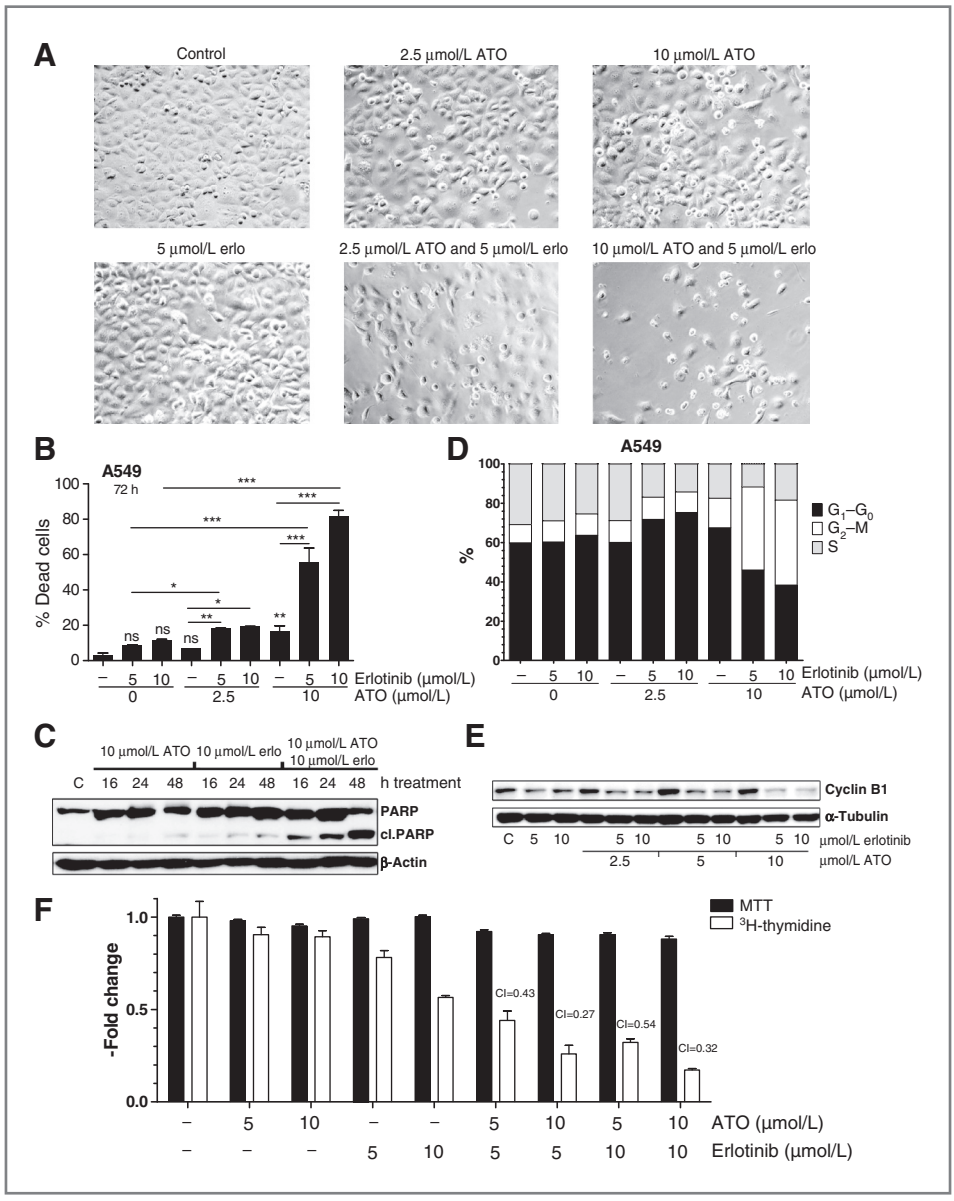


**Figure 3.** Impact of the ATO and erlotinib (erlo) drug combination on apoptosis induction, cell-cycle distribution, and DNA synthesis. A, phase-contrast microscopy pictures depict A549 cells after 72-hour treatment with ATO, erlotinib, or their combination at the indicated concentrations. B, apoptotic A549 cells were counted after ATO/erlotinib exposure for 72 hours on live cells stained with Hoechst 33258 and PI. The statistical significance was calculated using two-way ANOVA (*, $P < 0.05$; **, $P < 0.001$; ***, $P < 0.001$; ns, not significant). If not otherwise indicated, significance is given in comparison with control group. C, Western blot analysis of PARP cleavage in A549 cells was determined after 16-, 24-, and 48-hour treatment with the indicated drugs. D, the influence of ATO/erlotinib on cell-cycle distribution of A549 cells was determined by FACS analyses after 48-hour drug exposure. E, the impact of 24-hour drug exposure on the expression levels of cyclin B in A549 cells was determined by Western blot analysis. F, the impact of ATO and erlotinib on DNA synthesis was measured by $^3$H-thymidine incorporation after 24-hour incubation with the indicated drugs. Data are compared with those for cell viability determined by MTT assay. Respective CIs were calculated from radioactivity values of incorporated $^3$H-thymidine in cells treated with ATO/erlotinib as monotherapy and in combination.

less than 0.5. This block of DNA synthesis was accompanied by distinct changes in the cell-cycle distribution. Thus, cells treated with 10 μmol/L ATO and 5 or 10 μmol/L erlotinib for 24 hours revealed a distinct increase in the amount of $G_2$–M phase cells (from 12% to 22% and 26%, respectively; Supplementary Fig. S3D). This $G_2$–M phase arrest further increased to 42% and 43% of $G_2$–M phase cells, respectively, after 48-hour combination treatment (Fig. 3D). To further investigate the $G_2$–M arrest, cyclin B expression levels were analyzed. As shown in Fig. 3E, ATO monotreatment slightly enhanced cyclin B expression. In contrast, in cells treated with the drug combination cyclin B expression was dose-dependently decreased. These results are in accordance with the vitality data, where the drug combination was able to overcome the intrinsic resistance of A549 cells to ATO. This is of interest as there are several reports that ATO induces $G_2$–M arrest accompanied by a (p53/p21-dependent) decrease of cyclin B expression (31–33). Thus, the decrease of cyclin B1 only in the combination samples reflects the resensitization of A549 cells to ATO by erlotinib.

## Effects of the drug combination on DNA damage and repair

Besides its oncogenic activity, EGFR has recently been shown to promote DNA DSB repair by regulation of nonhomologous end-joining (34–36) as well as homologous end-joining (22, 37). To detect the amount of DNA DSBs after drug treatment, phosphorylation of H2AX histones was analyzed by immunostaining. Notably, at the concentrations used the amount of DSBs induced by the single agents was very minor reflecting the distinct

Published OnlineFirst April 2, 2013; DOI: 10.1158/1535-7163.MCT-13-0065



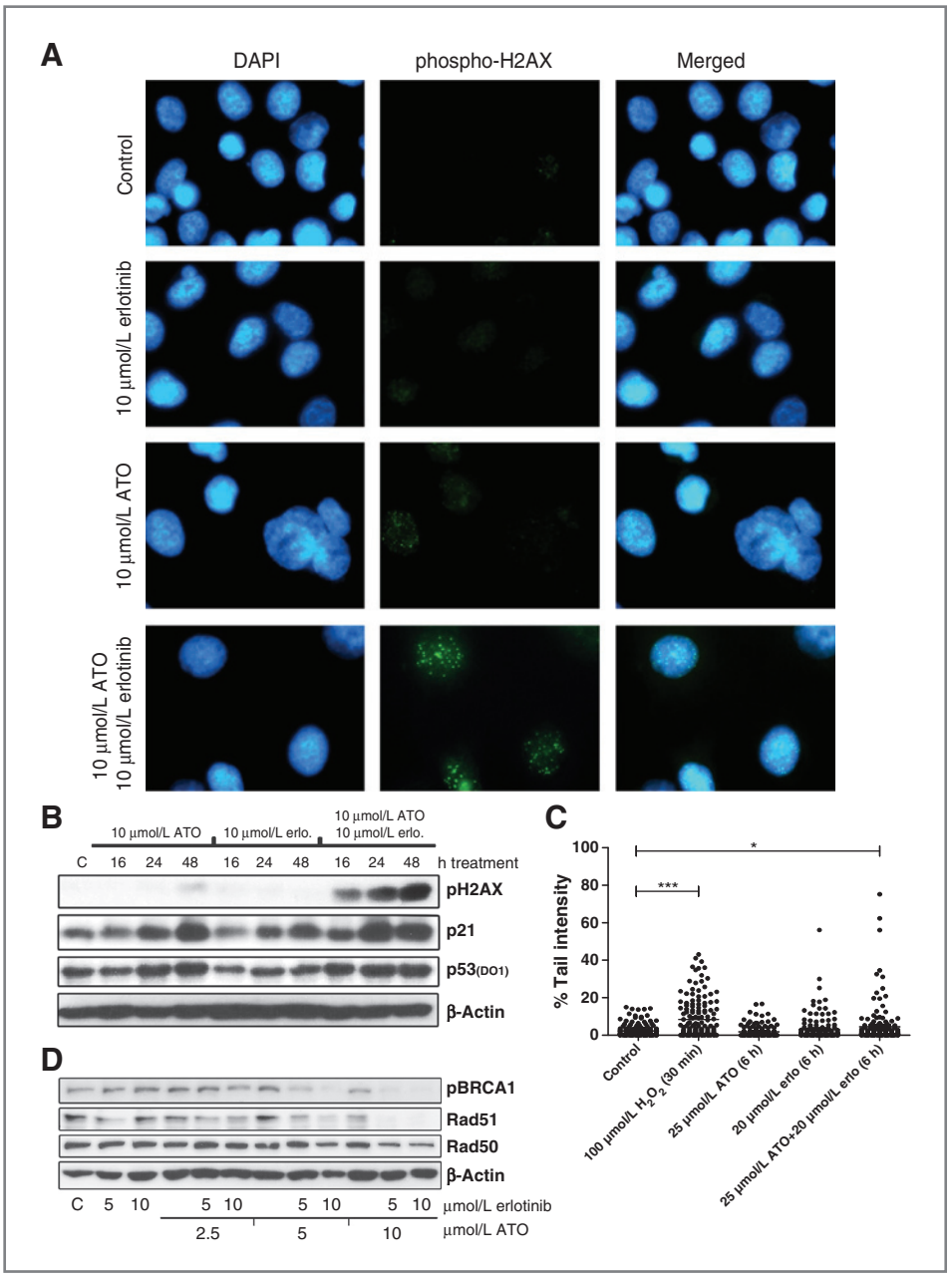


**Figure 4.** Influence of ATO/erlotinib on DNA damage and repair mechanisms in A549 cells. A, DNA DSBs were analyzed by detecting phospho-H2AX by immunofluorescence staining after 24-hour drug incubation at the indicated drug concentrations. B, phospho-H2AX, p21, and p53 levels detected by Western blotting after treatment with ATO/erlotinib for 16, 24, and 48 hours. C, DNA damage induced after 6-hour treatment of A549 cells with ATO and erlotinib (erlo) analyzed by comet assay. The percentage of tail intensity was scored (using Comet Assay IV image analysis system; Perceptive Instruments) in 150 randomly chosen comets of each sample (*, $P < 0.05$; ***, $P < 0.001$ calculated by one-way ANOVA). D, Western blot analysis of Rad51, Rad50, and pBRCA1 after 24-hour treatment with different drug concentrations.

therapy resistance of A549 cells against both drugs. In contrast, the drug combination considerably induced H2AX nuclear foci formation (Fig. 4A). Phosphorylation of H2AX was also confirmed by Western blotting after 16-, 24-, and 48-hour drug treatment (Fig. 4B). Also, the comet assays confirmed that the amount of DNA DSBs was significantly higher after 6-hour treatment with the drug combination setting than in the monotherapies (Fig. 4C). In accordance with these data, the combination of ATO with erlotinib led to an earlier induction of DNA damage response signals such as p53 and p21 (Fig. 4B). Noteworthy, the enhancement of DNA damage was not based on generation of hydroxyl or superoxide radicals upon combination of ATO with erlotinib (data not shown). In contrast, the drug combination led to distinct downregulation of the DNA DSB repair proteins Rad50 and Rad51 as well as a concentration-dependent decrease of BRCA1 phosphorylation (Fig. 4D).

### Synergistic activity of ATO and erlotinib *in vivo*

On the basis of the promising cell culture data, the efficacy of the ATO/erlotinib combination was tested against A549 xenografts in SCID mice. All treatment settings were well tolerated with no signs of toxicity, distress, or impact on activity/behavior parameters (data not shown). This is also reflected by the unaltered body

Published OnlineFirst April 2, 2013; DOI: 10.1158/1535-7163.MCT-13-0065



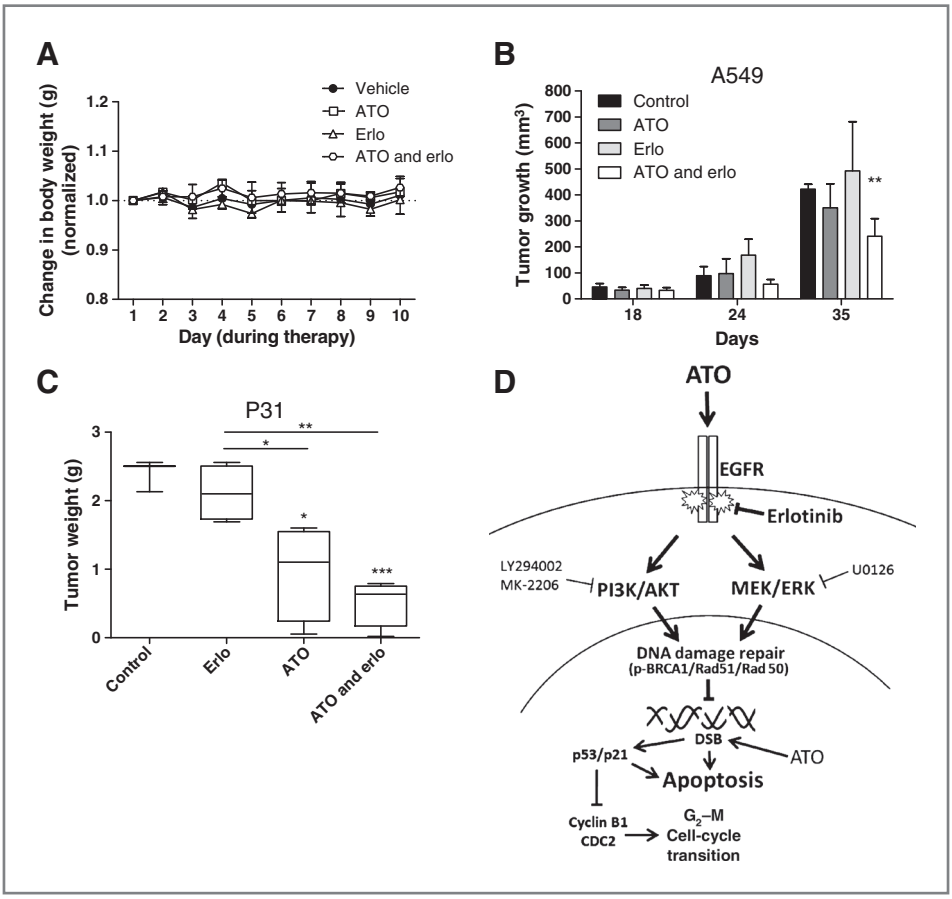


Figure 5. Impact of ATO and erlotinib (erlo) as monotherapy and in combination against human cancer xenografts in SCID mice. A, body weight of A549 xenografted mice ($n = 9$ per group) during therapy (2 weeks). B, effect of treatment on A549 tumor growth shown 18, 24, and 35 days after tumor injection. C, tumor weight after treatment of P31 xenografted mice at day 62. A549 and P31 xenografts were grown in Balb/c SCID mice and were treated with ATO (5 mg/kg; i.p., 5 consecutive d/wk) and/or erlotinib (25 mg/kg; orally, 5 consecutive d/wk) for 2 weeks. The statistical significance was calculated using one-way ANOVA (*, $P < 0.05$; **, $P < 0.01$; ***, $P < 0.001$). If not otherwise indicated, significance is given in comparison with control group. D, schematic representation of anticancer activity of ATO and tyrosine kinase inhibitors of the EGFR pathway.

weight in all experimental groups (Fig. 5A). With regard to the anticancer activity, due to the high resistance of A549 cells to the single agents, neither ATO nor erlotinib alone had any anticancer activity (Fig. 5B). In contrast, treatment with the drug combination resulted in significant reduction of tumor growth. In addition, the therapeutic efficacy of the new combination strategy was also tested in the orthotopic mesothelioma model P31 as this cell line was among the most responsive ones to ATO treatment in the MTT assays. Figure 5C depicts mean intraperitoneal tumor mass after 2 weeks of drug treatment (example pictures are shown in Supplementary Fig. S4). Also, in this xenograft, erlotinib monotherapy was found to be widely ineffective. In contrast, ATO monotreatment already had some growth inhibitory potential resulting in a significant reduction from a mean of 2.40 g to a mean of 0.96 g in the ATO-treated mice. Combination of ATO with erlotinib further enhanced this activity (to a mean of 0.52 g) emphasizing the potential of the treatment regimen.

## Discussion

Intrinsic and acquired resistance is still one of the major obstacles for successful anticancer therapy (38). Besides the development of new therapeutic approaches, one of the most promising options to improve treatment efficacy is the use of combination strategies (39). The anticancer activity of arsenic is well known and resulted in the recent approval of ATO against APL (1). However, the activity of ATO against solid cancer types is so far rather limited (8–11, 40). Some recent reports indicate that exposure to inorganic arsenic salts leads to activation of EGFR in nonmalignant as well as in malignant cells, for example, via c-Src kinase-mediated signals (14–19). In many solid tumor types, EGFR is one of the most important oncogenic receptor tyrosine kinases significantly supporting cell proliferation and survival via the MAPK and the PI3K/AKT axes, respectively (23, 41, 42). Consequently, we hypothesized that EGFR stimulation might play an important role in the resistance of solid cancer types against ATO. Indeed, our data show that inhibition of EGFR by erlotinib and gefitinib sensitizes diverse and even highly ATO-resistant solid tumor types of epithelial and mesenchymal origin against ATO, independent of their *TP53* or *RAS* mutation status (Supplementary Table S1). Moreover, our results suggest that these effects are mainly based on inhibition of EGFR-mediated DNA DSB repair associated with higher levels of DNA damage, subsequent cell-cycle arrest predominantly in $G_2$–M phase, and apoptosis induction. The synergistic activity of this drug combination was finally also confirmed using 2 human solid tumor xenograft models *in vivo*. A schematic

Published OnlineFirst April 2, 2013; DOI: 10.1158/1535-7163.MCT-13-0065



diagram illustrating the molecular mechanisms underlying this synergism is shown in Fig. 5D.

Notably, in our study, the synergism with ATO was not only observed for EGFR, but also for inhibitors of both major downstream signaling pathways namely MAPK and PI3K/AKT. This suggests that both pathways are involved in the protection of solid cancer cells against ATO. This is in agreement with earlier observations by other groups indicating that arsenic exposure leads to oxidative stress (1, 43) and subsequent activation of several redox-regulated signaling pathways including all 3 MAPK (43, 44) as well as the PI3K/AKT pathways (17) probably via activation of upstream EGFR (15). Accordingly, a synergistic activity of ATO with both PI3K/AKT and MEK/ERK inhibition has been frequently reported with a focus on hematologic malignancies (6, 17). However, only 3 reports on a synergism of ATO with EGFR inhibitors in cancer cells have been published so far. Ivanov and Hei (45) reported, in accordance with our data, enhanced ATO-mediated apoptosis induction by combination with the EGFR inhibitor AG1478 in EGFR-positive melanoma cells mainly via suppression of PI3K/AKT. In contrast, the synergism of ATO with gefitinib in APL cells was linked to enhanced cell differentiation by ROS-induced ERK activation (46). In hepatoma cells, suppression of transforming growth factor-β–induced factor as a consequence of EGFR inhibition was suggested as underlying mechanism (30).

The synergism between either EGFR or MAPK/PI3K inhibition and ATO has never been attributed to enhanced DNA damage based on reduced DSB repair so far. This is surprising, as both ATO and inhibition of EGFR and its downstream signals have been shown to result in compromised DNA repair processes (22, 34–37). Interestingly, we could not detect an enhanced generation of ROS in the drug combination despite synergistic induction of DNA DSBs and subsequent phosphorylation of H2AX. These data again suggest that reduced repair rather than enhanced damage caused a synergistic proliferation arrest and apoptosis induction by the ATO/erlotinib combination.

In general, the role of DNA damage in the anticancer activity of arsenic is controversially discussed (47, 48). Although it is widely assumed that the carcinogenic effects of chronic arsenic exposure are associated with arsenic-induced reactive species, which subsequently result in single-strand as well as DNA DSBs (47, 48), the underlying mechanisms seem to be complex. In addition, ROS-mediated DNA damage might be enhanced on the basis of downregulation of several ssDNA damage repair mechanisms by arsenic [e.g., decreased expression of the nucleotide excision repair (NER) proteins ERCC1, XPB, and XPF in lymphocytes from exposed individuals (49)]. Accordingly, a high number of indirect indications for enhanced DNA damage after arsenic exposure have been reported. For example, ATO induced base excision repair (BER)-specific DNA polymerase β (Polβ) activity indicative for ROS-mediated single-strand breaks (44). In addition, there is increasing evidence that especially deficiency in DNA DSB repair is associated with increased sensitivity to arsenic (50). Notably, besides multiple other functions, the EGFR pathway has been recently shown to be involved in the regulation of DNA DSB repair by positive regulation of both the homologous recombination as well as the nonhomologous end-joining (22, 37). Thus, activation of EGFR resulted in a decreased number of residual DNA DSBs, whereas the number of H2AX-positive DSB foci was clearly increased when EGFR was blocked by erlotinib in A549 and other lung cancer cell lines (22, 34). Moreover, erlotinib also attenuated DNA damage-induced Rad51 foci and resulted in cytoplasmic retention of BRCA1 (37), both essential components of the DSB repair machinery. With regard to our data, these findings strongly support the hypothesis that the synergism between ATO and EGFR inhibition observed in diverse solid tumor models is mainly caused by a synthetic lethal interaction between ATO-induced DNA damage and loss of EGFR-mediated repair capacity. Accordingly, the combination of ATO with erlotinib resulted in our hands in downregulation of the DNA DSB repair proteins Rad51 and Rad50 as well as reduced phosphorylation of BRCA1 associated with a significant increase of DNA DSBs, profound activation of pH2AX, and p53/p21–mediated cell-cycle arrest. The fact that this combination is strongly active even against the notoriously drug-resistant NSCLC model A549 indicates that such cross-talk might also exist for other DNA-damaging anticancer drugs. Moreover, we show for the first time that a synergistic anticancer activity of ATO is also achievable by coadministration of the EGFR inhibitor erlotinib *in vivo* when treating subcutaneous and orthotopic solid tumor xenografts. On the one hand, this implicates that ATO as anticancer agent might expand toward novel indications against solid tumors when combined with EGFR inhibitors. On the other hand, it has to be considered that EGFR tyrosine kinase inhibitors such as erlotinib have been successfully used predominantly in tumors harboring constitutively activating EGFR-mutations (23). However, the widespread sensitization toward erlotinib by coadministration of ATO reported in this study both *in vitro* and *in vivo* was observed in cell models without EGFR-activating mutations. Thus, the combination with ATO might expand the beneficial application of EGFR inhibitors toward patient populations harboring cancers with wild-type EGFR background. Moreover, it has been hypothesized that EGFR activation might play a role in the carcinogenic effects of chronic exposure to arsenic (16). Thus, one might hypothesize that combination with EFGR inhibitors might not only sensitize cancer cells toward ATO but at the same time reduce the potential procarcinogenic effects of ATO cancer therapy.

Summarizing, our data suggest that the combination of ATO with erlotinib or other EGFR inhibitors might be a promising strategy to enhance the susceptibility of solid cancer cells to ATO treatment and, thus, overcome drug resistance. This is of special interest as both, ATO as well as erlotinib, are already in clinical use, which facilitates the performance of clinical combination trials.

Published OnlineFirst April 2, 2013; DOI: 10.1158/1535-7163.MCT-13-0065



## Disclosure of Potential Conflicts of Interest

No potential conflicts of interest were disclosed.

## Authors' Contributions

**Conception and design:** K. Kryeziu, W. Berger, P. Heffeter
**Development of methodology:** K. Kryeziu, U. Jungwirth
**Acquisition of data (provided animals, acquired and managed patients, provided facilities, etc.):** K. Kryeziu, M.A. Hoda, F. Ferk, P. Heffeter
**Analysis and interpretation of data (e.g., statistical analysis, biostatistics, computational analysis):** K. Kryeziu, U. Jungwirth, P. Heffeter
**Writing, review, and/or revision of the manuscript:** K. Kryeziu, U. Jungwirth, M.A. Hoda, S. Knasmüller, C. Karnthaler-Benbakka, C.R. Kowol, W. Berger, P. Heffeter
**Administrative, technical, or material support (i.e., reporting or organizing data, constructing databases):** M.A. Hoda, C. Karnthaler-Benbakka, C.R. Kowol, P. Heffeter
**Study supervision:** W. Berger, P. Heffeter

## Acknowledgments

The authors thank Irene Herbacek for FACS measurements, Paul Breit for photography, Christian Balcarek for skillful assistance, and Gerhard Zeitler for animal care.

## Grant Support

This work was supported by the "Herzfelder Familienforschung" (P. Heffeter), "Fonds der Stadt Wien für innovative interdisziplinäre Krebsforschung" (P. Heffeter and C.R. Kowol).

The costs of publication of this article were defrayed in part by the payment of page charges. This article must therefore be hereby marked *advertisement* in accordance with 18 U.S.C. Section 1734 solely to indicate this fact.

Received January 24, 2013; revised March 11, 2013; accepted March 27, 2013; published OnlineFirst April 2, 2013.

## References

1. Jungwirth U, Kowol CR, Keppler BK, Hartinger CG, Berger W, Heffeter P. Anticancer activity of metal complexes: involvement of redox processes. Antioxid Redox Signal 2011;15:1085–127.
2. Kito M, Akao Y, Ohishi N, Yagi K, Nozawa Y. Arsenic trioxide-induced apoptosis and its enhancement by buthionine sulfoximine in hepatocellular carcinoma cell lines. Biochem Biophys Res Commun 2002;291:861–7.
3. Miller WH Jr, Schipper HM, Lee JS, Singer J, Waxman S. Mechanisms of action of arsenic trioxide. Cancer Res 2002;62:3893–903.
4. Davison K, Mann KK, Miller WH Jr. Arsenic trioxide: mechanisms of action. Semin Hematol 2002;39:3–7.
5. Emadi A, Gore SD. Arsenic trioxide—an old drug rediscovered. Blood Rev 2010;24:191–9.
6. Takahashi S. Combination therapy with arsenic trioxide for hematological malignancies. Anticancer Agents Med Chem 2010;10:504–10.
7. Zhang X, Su Y, Zhang M, Sun Z. Opposite effects of arsenic trioxide on the Nrf2 pathway in oral squamous cell carcinoma *in vitro* and *in vivo*. Cancer Lett 2012;318:93–8.
8. Lin CC, Hsu C, Hsu CH, Hsu WL, Cheng AL, Yang CH. Arsenic trioxide in patients with hepatocellular carcinoma: a phase II trial. Invest New Drugs 2007;25:77–84.
9. Vuky J, Yu R, Schwartz L, Motzer RJ. Phase II trial of arsenic trioxide in patients with metastatic renal cell carcinoma. Invest New Drugs 2002;20:327–30.
10. Kim KB, Bedikian AY, Camacho LH, Papadopoulos NE, McCullough C. A phase II trial of arsenic trioxide in patients with metastatic melanoma. Cancer 2005;104:1687–92.
11. Kindler HL, Aklilu M, Nattam S, Vokes EE. Arsenic trioxide in patients with adenocarcinoma of the pancreas refractory to gemcitabine a phase II trial of the University of Chicago Phase II Consortium. Am J Clin Oncol 2008;31:553–6.
12. Subbarayan PR, Lima M, Ardalan B. Arsenic trioxide/ascorbic acid therapy in patients with refractory metastatic colorectal carcinoma: a clinical experience. Acta Oncol 2007;46:557–61.
13. Chervona Y, Arita A, Costa M. Carcinogenic metals and the epigenome: understanding the effect of nickel, arsenic, and chromium. Metallomics 2012;4:619–27.
14. Eblin K. Potential clinical significance of EGFR-mediated signaling following inorganic arsenic exposure in human lung. Toxicol Sci 2009;109:169–71.
15. Carpenter RL, Jiang BH. Roles of EGFR, PI3K, AKT, and mTOR in Heavy Metal-Induced Cancer. Curr Cancer Drug Targets 2013 Jan 2. [Epub ahead of print].
16. Simeonova PP, Wang S, Hulderman T, Luster MI. c-Src-dependent activation of the epidermal growth factor receptor and mitogen-activated protein kinase pathway by arsenic. Role in carcinogenesis. J Biol Chem 2002;277:2945–50.
17. Kodigepalli KM, Dutta PS, Bauckman KA, Nanjundan M. SnoN/SkiL expression is modulated via arsenic trioxide-induced activation of the PI3K/AKT pathway in ovarian cancer cells. FEBS Lett 2012;587:5–16.
18. Liu ZM, Huang HS. $As_2O_3$-induced c-Src/EGFR/ERK signaling is via Sp1 binding sites to stimulate p21WAF1/CIP1 expression in human epidermoid carcinoma A431 cells. Cell Signal 2006;18:244–55.
19. Andrew AS, Mason RA, Memoli V, Duell EJ. Arsenic activates EGFR pathway signaling in the lung. Toxicol Sci 2009;109:350–7.
20. Tseng HY, Liu ZM, Huang HS. NADPH oxidase-produced superoxide mediates EGFR transactivation by c-Src in arsenic trioxide-stimulated human keratinocytes. Arch Toxicol 2012;86:935–45.
21. Sibilia M, Kroismayr R, Lichtenberger BM, Natarajan A, Hecking M, Holcmann M. The epidermal growth factor receptor: from development to tumorigenesis. Differentiation 2007;75:770–87.
22. Myllynen L, Rieckmann T, Dahm-Daphi J, Kasten-Pisula U, Petersen C, Dikomey E, et al. In tumor cells regulation of DNA double strand break repair through EGF receptor involves both NHEJ and HR and is independent of p53 and K-Ras status. Radiother Oncol 2011;101:147–51.
23. Gazdar AF. Epidermal growth factor receptor inhibition in lung cancer: the evolving role of individualized therapy. Cancer Metastasis Rev 2010;29:37–48.
24. Chou TC, Talalay P. Quantitative analysis of dose-effect relationships: the combined effects of multiple drugs or enzyme inhibitors. Adv Enzyme Regul 1984;22:27–55.
25. Berger W, Elbling L, Minai-Pour M, Vetterlein M, Pirker R, Kokoschka EM, et al. Intrinsic MDR-1 gene and P-glycoprotein expression in human melanoma cell lines. Int J Cancer 1994;59:717–23.
26. Heffeter P, Pirker C, Kowol CR, Herrman G, Dornetshuber R, Miklos W, et al. Impact of terminal dimethylation on the resistance profile of alpha-N-heterocyclic thiosemicarbazones. Biochem Pharmacol 2012;83:1623–33.
27. Tice RR, Agurell E, Anderson D, Burlinson B, Hartmann A, Kobayashi H, et al. Single cell gel/comet assay: guidelines for *in vitro* and *in vivo* genetic toxicology testing. Environ Mol Mutagen 2000;35:206–21.
28. Heffeter P, Popovic-Bijelic A, Saiko P, Dornetshuber R, Jungwirth U, Voevodskaya N, et al. Ribonucleotide reductase as one important target of [Tris(1,10-phenanthroline)lanthanum(III)] trithiocyanate (KP772). Curr Cancer Drug Targets 2009;9:595–607.
29. Hoda MA, Mohamed A, Ghanim B, Filipits M, Hegedus B, Tamura M, et al. Temsirolimus inhibits malignant pleural mesothelioma growth *in vitro* and *in vivo*: synergism with chemotherapy. J Thorac Oncol 2011;6:852–63.
30. Liu ZM, Tseng JT, Hong DY, Huang HS. Suppression of TG-interacting factor sensitizes arsenic trioxide-induced apoptosis in human hepatocellular carcinoma cells. Biochem J 2011;438:349–58.
31. Zhao S, Tsuchida T, Kawakami K, Shi C, Kawamoto K. Effect of $As_2O_3$ on cell cycle progression and cyclins D1 and B1 expression in two glioblastoma cell lines differing in p53 status. Int J Oncol 2002;21:49–55.
32. Chao JI, Hsu SH, Tsou TC. Depletion of securin increases arsenite-induced chromosome instability and apoptosis via a p53-independent pathway. Toxicol Sci 2006;90:73–86.

Published OnlineFirst April 2, 2013; DOI: 10.1158/1535-7163.MCT-13-0065




33. Seol JG, Park WH, Kim ES, Jung CW, Hyun JM, Kim BK, et al. Effect of arsenic trioxide on cell cycle arrest in head and neck cancer cell line PCI-1. Biochem Biophys Res Commun 1999;265:400–4.
34. Kriegs M, Kasten-Pisula U, Rieckmann T, Holst K, Saker J, Dahm-Daphi J, et al. The epidermal growth factor receptor modulates DNA double-strand break repair by regulating non-homologous end-joining. DNA Repair (Amst) 2010;9:889–97.
35. Mukherjee B, Choy H, Nirodi C, Burma S. Targeting nonhomologous end-joining through epidermal growth factor receptor inhibition: rationale and strategies for radiosensitization. Semin Radiat Oncol 2010;20:250–7.
36. Toulany M, Lee KJ, Fattah KR, Lin YF, Fehrenbacher B, Schaller M, et al. Akt promotes post-irradiation survival of human tumor cells through initiation, progression, and termination of DNA-PKcs-dependent DNA double-strand break repair. Mol Cancer Res 2012;10:945–57.
37. Li L, Wang H, Yang ES, Arteaga CL, Xia F. Erlotinib attenuates homologous recombinational repair of chromosomal breaks in human breast cancer cells. Cancer Res 2008;68:9141–6.
38. Heffeter P, Jungwirth U, Jakupec M, Hartinger C, Galanski M, Elbling L, et al. Resistance against novel anticancer metal compounds: differences and similarities. Drug Resist Updat 2008;11:1–16.
39. Al-Lazikani B, Banerji U, Workman P. Combinatorial drug therapy for cancer in the post-genomic era. Nat Biotechnol 2012;30:679–92.
40. Smith MA, Kang MH, Reynolds CP, Kurmasheva RT, Alexander D, Billups CA, et al. Evaluation of arsenic trioxide by the pediatric preclinical testing program with a focus on Ewing sarcoma. Pediatr Blood Cancer 2012;59:753–5.
41. McCubrey JA, Steelman LS, Chappell WH, Abrams SL, Wong EW, Chang F, et al. Roles of the Raf/MEK/ERK pathway in cell growth, malignant transformation and drug resistance. Biochim Biophys Acta 2007;1773:1263–84.
42. Cargnello M, Roux PP. Activation and function of the MAPKs and their substrates, the MAPK-activated protein kinases. Microbiol Mol Biol Rev 2011;75:50–83.
43. Hartwig A. Metal interaction with redox regulation: an integrating concept in metal carcinogenesis? Free Radic Biol Med 2012;55C: 63–72.
44. Herbert KJ, Snow ET. Modulation of arsenic-induced epidermal growth factor receptor pathway signalling by resveratrol. Chem Biol Interact 2012;198:38–48.
45. Ivanov VN, Hei TK. Combined treatment with EGFR inhibitors and arsenite upregulated apoptosis in human EGFR-positive melanomas: a role of suppression of the PI3K-AKT pathway. Oncogene 2005;24: 616–26.
46. Noh EK, Kim H, Park MJ, Baek JH, Park JH, Cha SJ, et al. Gefitinib enhances arsenic trioxide ($As_2O_3$)-induced differentiation of acute promyelocytic leukemia cell line. Leuk Res 2010;34:1501–5.
47. Martinez VD, Vucic EA, Adonis M, Gil L, Lam WL. Arsenic biotransformation as a cancer promoting factor by inducing DNA damage and disruption of repair mechanisms. Mol Biol Int 2011;2011: 718974.
48. Jungwirth U, Kowol CR, Hartinger C, Keppler BK, Berger W, Heffeter P. Anticancer activity of metal complexes: involvement of redox processes. Antioxid Redox Signal 2011;15:1085–127.
49. Andrew AS, Karagas MR, Hamilton JW. Decreased DNA repair gene expression among individuals exposed to arsenic in United States drinking water. Int J Cancer 2003;104:263–8.
50. Ying S, Myers K, Bottomley S, Helleday T, Bryant HE. BRCA2-dependent homologous recombination is required for repair of arsenite-induced replication lesions in mammalian cells. Nucleic Acids Res 2009;37:5105–13.